Friction

Research Article

The study of quantitative friction damage models at the interventional catheter–vascular tissue interface

Chengxiong Lin[1,2,3,✉], Huilu Yuan[3,4,5], Chengyong Wang[4,5,✉]

Cite this article: Lin CX, Yuan HL, Wang CY. *Friction* 2026, **14**(8): 9441194. https://doi.org/10.26599/FRICT.2025.9441194

ABSTRACT: Vascular interventional surgery is a minimally invasive treatment. This method involves introducing catheters, guidewires, and other precision instruments into the human body to locally diagnose and treat internal diseases. However, mechanical contact, such as friction, compression, and collision, inevitably occurs during the intervention process. This can cause tissue damage. Currently, mechanical damage to vascular tissues is evaluated primarily in qualitative terms, which limits accurate reflection of both the extent of tissue damage and its influencing factors. This paper specifically studies friction injury between interventional catheters and vascular tissues. This study develops the first quantification model of injury between catheters and blood vessels. The results revealed that increases in the normal force led to increased coefficients of friction (COF) and greater energy dissipation between the friction head and vascular tissue. In contrast, varying speeds produced a trend where the COF and energy dissipation first increased and then decreased. A quantitative evaluation system for vascular tissue injury was established on the basis of indicators such as endothelial cells, glycoproteins, curled tissues, and intimal thickness on the vascular surface. Using this system, damage scores and damage grades were assigned to surface injuries in friction experiments. Pearson correlation analysis revealed a strong correlation between the COF and injury score. The link between the normal load and sliding velocity was even greater than that between the friction time and injury score. These experimental results lay the foundation for quantitative mechanical damage evaluation. They enable the mapping of relationships between mechanical factors and tissue damage.

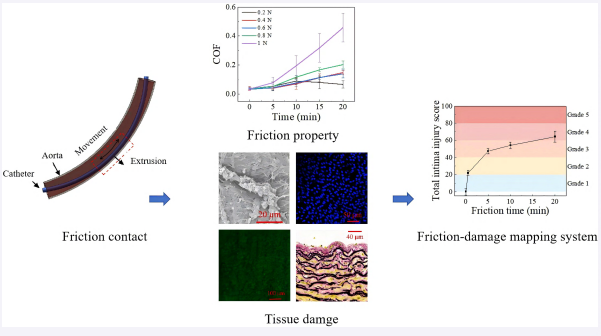

KEYWORDS: friction; vascular catheter; mechanical damage; quantitative evaluation system

1 Introduction

Vascular interventional surgery is a surgical method that treats cardiovascular diseases *in vivo* via a catheter or guide wire, offering advantages such as minimal trauma, high precision, multiple indications, straightforward operation, and rapid postoperative recovery. It has become the mainstream method for treating vascular diseases [1–4]. More than 200 million catheters are used for vascular intervention worldwide every year [5]. However, in both traditional doctor operation and digital control of vascular surgery robots, the following problems still exist during the process of X-ray-assisted catheter intervention [6, 7]: (1) The contact force and other information between the catheter and the vascular tissue cannot be obtained in real time during the process of the catheter passing through the blood vessel, and the lack of force feedback information leads to improper operation and tissue damage. (2) Due to the irregular size and structure of blood vessels, complications such as bleeding, intimal tearing, arterial spasm, rapid heart rate, and catheter knot are prone to occur when the catheter is frequently pushed, pulled, squeezed, and rotated in the blood vessel. (3) The sudden release of energy accumulated due to deformation at the front end of the catheter or the flexible tube during surgery will have an impact on the tissue, increasing the risk of vascular damage or even tearing. Therefore, although vascular intervention is widespread, complications associated with frictional injuries limit its clinical effectiveness [8, 9].

To understand the frictional damage mechanism between the interventional catheter and blood vessels and improve the safety and accuracy of surgery, scholars have conducted numerous

[1] Key Laboratory of Metallurgical Equipment and Control Technology (Ministry of Education), Wuhan University of Science and Technology, Wuhan 430081, China. [2] Hubei Key Laboratory of Mechanical Transmission and Manufacturing Engineering, Wuhan University of Science and Technology, Wuhan 430081, China. [3] Institute of Biological and Medical Engineering, Guangdong Academy of Sciences, Guangzhou 510316, China. [4] State Key Laboratory of High-Performance Tools, Guangdong University of Technology, Guangzhou 510006, China. [5] Guangdong Provincial Key Laboratory of Minimally Invasive Surgical Instruments and Manufacturing Technology, Guangdong University of Technology, Guangzhou 510006, China.

✉ Corresponding authors. E-mail: C. Lin, lcx3625@wust.edu.cn; C. Wang, cywang@gdut.edu.cn

Received: July 23, 2025; Revised: October 15, 2025; Accepted: November 19, 2025

studies [10–12]. Takashima et al. [13] employed frictional experiments and numerical analysis to investigate the contact behavior between blood vessels and catheters and reported that the coefficients of friction (COF) tended to first increase but then decrease with increasing contact angle. The numerical analysis results revealed that the difference in blood vessel parameters affected the movement trajectory of catheters in the surgical simulator. Prokopovich et al. [14, 15] tested the COF between the catheter and vascular tissue through face-on contact. Owing to high surface roughness, the static friction coefficient and dynamic friction coefficient of the arterial tissue were greater than those of the venous tissue, and the blood had good lubricity. Bostan et al. [16] reported that the COF between the catheter and the blood vessel was negatively correlated with the normal force, and interfacial friction resulted in significant changes in the orientation of both collagen fibers and elastic fibers. Lin et al. [17] studied the frictional properties of vessels with different curvatures and reported that the COF decreased with increasing normal force and increased with increasing moving speed. There was a corresponding relationship between the curvature, stiffness, contact area, and COF of the vessel, and the glycocalyx on the vessel had a mechanical lubrication effect at the macroscopic level. Wang et al. [18] conducted a study on the sliding friction between the end of a dialysis catheter and venous vessels and reported that the COF was positively correlated with the surface roughness of the catheter and that a highly rough surface might cause chronic mechanical friction damage to the intima of the central vein. At the cellular level, Dunn et al. [19] reported that the macroscopic COF between a glass needle and monolayer arterial endothelial cells was between 0.03 and 0.06 and preliminarily summarized the biological effects of frictional stress by evaluating damage to the cell area before and after friction.

Furthermore, the investigation of the frictional mechanism of vascular tissue damage can aid in determining the relationship between mechanical action and tissue damage, thereby providing a theoretical model for reducing tissue damage [20–23]. Dellimore et al. [24] used attenuated total internal reflection infrared spectroscopy to evaluate mechanical/frictional damage to the vascular wall, and the results revealed that the COF and degree of damage to blood vessels increased with increasing number of reciprocating frictions and that the absorbance gradually decreased. Bostan et al. [16] utilized second-harmonic imaging and two-photon excited fluorescence technology to investigate the orientation and quantity of vascular fibers. The results showed that after the friction experiment, the elastic fibers and collagen fibers in the blood vessels initially exhibited a significant change in orientation. With increasing recovery time, the fiber orientation gradually returned to the original state. Cheheltani et al. [25] and Votteler et al. [26] investigated extracellular matrix remodeling and degradation of arterial tissue via infrared and Raman spectroscopy, respectively. The results revealed that the Raman signal intensity and infrared spectrum signal significantly changed before and after collagen fiber degradation. Lin et al. [27–29] employed fluorescence microscopy and scanning electron microscopy to investigate the frictional damage between the modified catheter and blood vessels. The results revealed a decrease in mucin and the number of cells on the blood vessels after the friction of the modified catheter was reduced, and there was no prominent fold in the intima of the artery. In addition, Hofmann et al. [30] evaluated the degree of damage to corneal samples at the microscopic scale via ImageJ software, and the results revealed that the frictional energy between the lens and the cornea was positively correlated with the degree of tissue damage.

Current research on mechanical injury to vascular tissue has focused primarily on the frictional mechanism. Injury to vascular tissue, including tissue sections, infrared spectroscopy, Raman spectroscopy, and scanning electron microscopy, is assessed mainly through qualitative evaluation and comparison. The changes in vascular tissue corresponding to different contact conditions and the determining factors among various injuries are still unclear. Therefore, this paper specifically researched frictional injury between interventional catheters and vascular tissues and constructed a quantification model of this injury for the first time. First, the friction mechanism between the catheter and the vascular intima was analyzed under various factors, including friction time, normal force, and sliding velocity. Second, vascular tissue injury was analyzed via friction experiments, and a quantitative system for evaluating vascular injury was constructed. Finally, the mapping relationship between mechanical friction and tissue injury was expounded, revealing the friction injury mechanism of the interventional catheter to vascular tissue during the operation. The above experimental results lay the foundation for quantitative mechanical damage evaluation, enabling the construction of a mapping relationship between mechanical factors and tissue damage.

2 Materials and methods

2.1 Sample preparation

The tissue samples used in this study were derived from the aorta of pigs. They were obtained from the slaughterhouse on the day of the experiment. Intact aortas were sent to the laboratory within 2 h after death, and the surface mucosa was treated before the experiment was conducted within 4 h to avoid dehydration and deterioration. The processing procedure for arterial tissue was introduced in previous publications by the research group [17]. Briefly, the mucosa and other tissues on the outer surface of the aorta were removed to ensure the flatness of the sample. Then, samples were taken along the central axis of the aorta for the friction experiment. The tissue samples used for the friction experiment were 50 mm × 30 mm in length and width, with the thickness of the aortic wall ranging from 1.5 to 3 mm. To simulate real physiological conditions, this study used a blood substitute solution to create a vascular contact environment in friction experiments involving isolated vascular tissues. The formulation of the blood substitute solution is shown in Table 1.

2.2 Friction platform preparation

The interfacial friction test platform between the catheters and blood vessels was composed of a multifunctional friction and wear testing machine, a vascular fixation stage, and a friction ball, as shown in Fig. 1. The friction experiment in the present study was conducted on a friction and wear testing machine (UMT-

Table 1 Components of the blood substitute solution

Reagent	Concentration (w/v)	Brand	Component proportion
PBS solution	—	Tetrad organism	90%
Pig serum	Hemoglobin ≤ 0.02% Protein 4.5%–6.0%	Biosharp	10%

Tribolab, Bruker, USA), and the linear reciprocating mode in constant force mode was adopted to simulate the push–pull motion at the interventional catheter/aorta interface [29]. The corresponding friction test parameters were set as follows: the unidirectional sliding stroke was 15 mm; the sliding speeds were 1, 3, 5, 7, and 9 mm/s; the normal forces were 0.2, 0.4, 0.6, 0.8, and 1.0 N; and the reciprocating cycles were 1, 50, 100, 150, and 200. The vascular fixation stage was designed and self-processed via three-dimensional (3D) modeling software for the fixation of vascular tissues and simulation of the vascular environment. The materials of the friction ball were the same as those of standard commercial catheters, namely, polytetrafluoroethylene (PTFE; ϕ16 mm, PA66, Forsoow, China). Two parts were used: The outside end was a hemispherical friction head for the friction experiments, and the inner end was the part where the friction head connected to the friction testing machine, which was made of a metal material. The relevant material properties are detailed in Table 2.

2.3 Treatment of friction samples

After the aortic samples underwent friction experiments, they were fixed to maintain their integrity and structural stability for subsequent research. Specifically, these samples were immersed in paraformaldehyde (PFA) solution and fixed at 4 °C for 24 h. The samples were subsequently washed three times with a phosphate-buffered saline (PBS) solution to remove excess fixative. Finally, the samples were immersed in PBS solution and stored in a 4 °C refrigerator for future damage characterization studies. Within the friction area and the nonfriction area, 5 mm × 5 mm tissue samples were taken for dehydration and staining to evaluate the surface morphology and structure. Additionally, 3 mm × 20 mm tissue samples were taken from the friction area for histologic sectioning and staining to assess changes in the vascular intima.

2.3.1 *Fluorescence staining*

4',6-Diamidine-2'-phenylindole dihydrochloride (DAPI; CAS: 28718-90-3, Merck, Germany) and concanavalin A (ConA; CAS: 11028-71-0, Sigma-Aldrich, Germany) were used to stain the cell nucleus and glycocalyx of the blood vessels, respectively. DAPI can strongly bind to DNA and is commonly used for observing the cell nucleus. In contrast, ConA can specifically bind to specific structures of various sugars, glycoproteins, and glycolipids and is thus used to characterize glycoproteins and other sugar-containing substances on blood vessels (such as the glycocalyx). The operation steps were as follows: (1) PBS was used to remove impurities, and additional PFA solution was added to the samples; (2) a mixture of ConA (2 mg/mL) and DAPI (2 mg/mL) was added, and the tissue sample was immersed in the dark at room temperature for 30 min; (3) the samples were washed with PBS three times for 10 min each to remove the staining solution; (4) the fluorescence of the samples was observed under an inverted fluorescence microscope (ConA appeared green, and the DAPI appeared blue; IX73 Olympus, Japan); (5) ImageJ software was used to analyze the fluorescence intensity of glycoproteins and cell nuclei statistically.

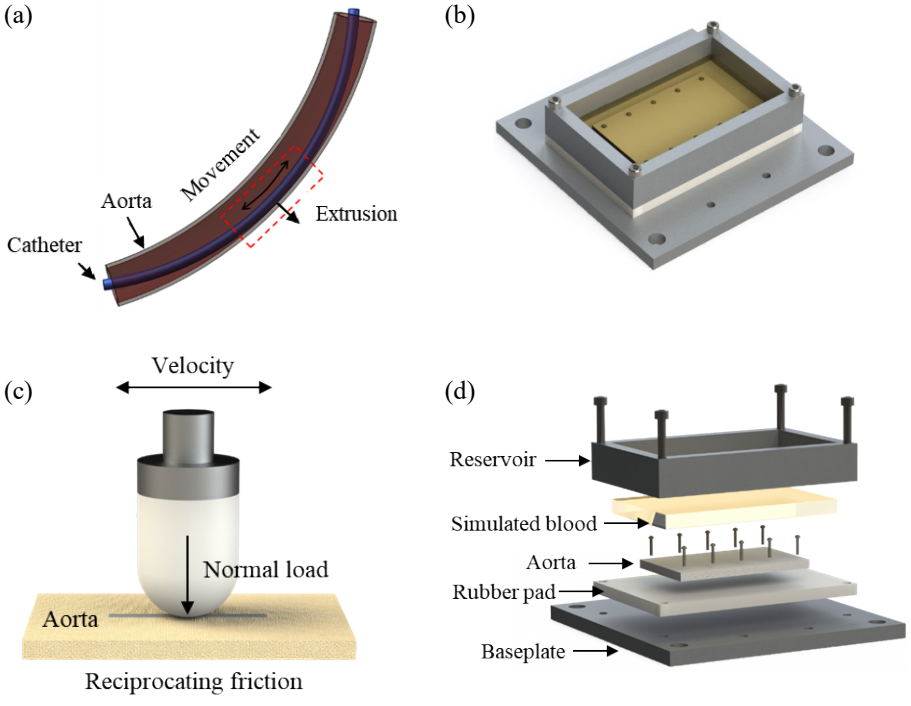

Fig. 1 Interfacial friction test platform between catheters and blood vessels. Schematic diagram of (a) interface contact, (b) sample fixing stage on UMT-tribolab, (c) frictional head, and (d) specific structure of fixing stage.

Table 2 The material properties of the friction ball head

Material	Diameter (mm)	Elasticity modulus (MPa)	Poisson's ratio	Picture
PTFE	16	674	0.475	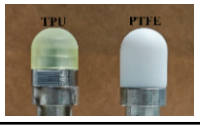

2.3.2 Sample topography

The surface morphology of the samples before and after the friction test was assessed with a scanning electron microscope (SEM; Phenom Prox G7, the Netherlands). The samples were first cut from the friction area and the nonfriction area. The samples were subsequently immersed in ethanol solutions of 50%, 70%, 80%, 90%, 95%, and 100% concentrations for gradient dehydration. After that, the samples were placed in a well-ventilated area for drying for more than 1 h and sprayed with gold in a vacuum environment. Finally, the samples were observed via SEM, and the extracted tissue was statistically analyzed via ImageJ software.

2.3.3 Histological section

Histological sectioning is one of the most fundamental and widely used staining techniques in histology and pathology and can reveal the morphological structure of cells and tissues. Elastic Van Gieson (EVG) staining is used to visualize elastic fibers and collagen fibers in tissues, with elastic fibers stained black and collagen fibers stained red. The steps for histologic sectioning were as follows: First, the samples were trimmed to the appropriate width; then, the tissue sections were stained with EVG according to the user manuals after routine dehydration, embedding, sectioning, mounting, and dewaxing; subsequently, the tissue sections were dehydrated and sealed on microscope slides for long-term preservation; and finally, the sample tissue in the sections was observed via a biological microscope (BX63, Olympus, Japan). As shown in Fig. 2, the vascular tissue is composed of the inner layer (endothelium), the middle layer (media), and the outer layer (adventitia) from the inside to the outside.

2.4 Damage assessment system

To evaluate the degree of damage to vascular tissues after the friction experiment, a damage assessment system was established to assess vascular tissue damage. It can not only intuitively display the severity of tissue damage but also facilitate the analysis and comparison of the influences of different damage factors. The damage assessment system primarily includes data processing methods, statistical analysis methods, and weight determination methods, among others.

2.4.1 Data standardization

When the order of magnitude of the selected indicators for damage assessment varies significantly, it is essential to standardize the measurement data and convert the quantified data into standardized units to minimize errors among the indicators. Among these methods, the most common is the range standardization method, which subtracts the minimum value from the actual measurement data and then divides the resulting data by the range of the data. The calculation expression is in Eq. (1) [31]:

$$\text{Standardized value} = \frac{\text{Measured value} - \text{Minimum value}}{\text{Maximum value} - \text{Minimum value}} \tag{1}$$

2.4.2 Hierarchical analysis method

The hierarchical analysis method is a commonly used calculation method for assigning weights to different indicators, enabling a comprehensive evaluation of a specific object. The analysis process included the following steps [32–34]: (1) A hierarchical network structure diagram was established on the basis of the decision-making objective (Fig. S1 in the Electronic Supplementary Material (ESM)). (2) With the 1–3–5–7–9 evaluation method in the hierarchical analysis method (Table S1 in the ESM), the superiority and inferiority judgment matrix for the subobjectives of the first layer was then constructed (Table S2 in the ESM). (3) The weights of the subobjectives were calculated, and whether the obtained weights were logical was verified. The specific calculation formula was as follows.

First, the initial weights of the subgoals are calculated as Eq. (2):

$$w_i' = \sqrt[m]{a_{i1}a_{i2}\cdots a_{im}} \tag{2}$$

where a_{ij} means the valuer in 1–3–5–7 layered analysis, i represents the serial number of the subobjective, w_i' is the initial weight of the i-th subobjective, and m is the number of subobjectives.

The initial weights of the subobjectives are normalized to obtain the normalized weight coefficients. The calculation equation is as Eq. (3):

$$w_i = w_i' / \sum_{i=1}^{m} w_i' \tag{3}$$

The consistency index (CI) is used to determine whether the weights assigned to subobjectives are logical. The calculation formula of the CI is as Eq. (4):

$$\text{CI} = (\lambda_{\max} - m)/(m-1) \tag{4}$$

where $\lambda_{\max}$ is the maximum eigenvalue, and m is the eigenvalue of the pairwise comparison judgment preference matrix of the subobjectives at this layer.

Finally, the comprehensive score index is calculated. The calculation formula is as Eq. (5):

$$\text{GI} = \sum_{1}^{m} C_i Z_i \tag{5}$$

where GI is the final comprehensive score, C_i is the weight (combined weight), and Z_i represents the standardized data of the i-th evaluation index.

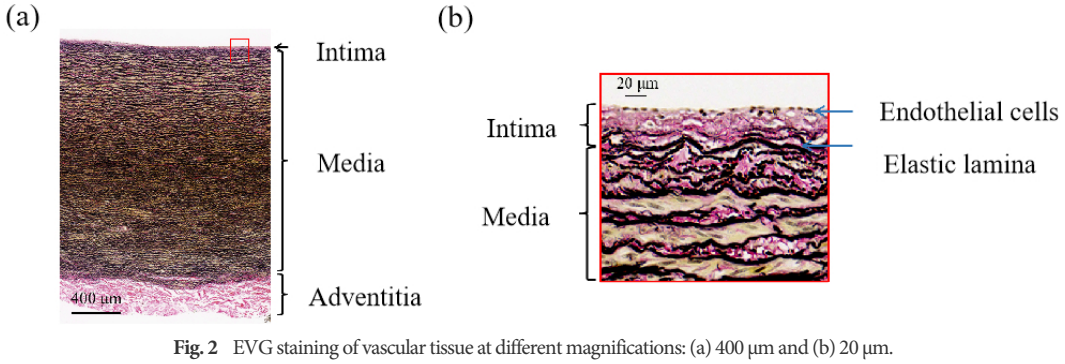

Fig. 2 EVG staining of vascular tissue at different magnifications: (a) 400 μm and (b) 20 μm.

3 Results

3.1 The dependence of friction time

Figures 3(a) and 3(b) show the typical trends of the COF over time during the unidirectional sliding of the friction ball head on the vascular surface, where numbers 1–3 represent different friction states. At the beginning of movement, the friction head and the vascular surface are in a relatively static state. As the friction head starts to move initially, static friction behavior occurs at the friction ball-vessel tissue interface, and the COF increases rapidly over time during this stage. During the process where the COF increases from zero to the maximum static friction coefficient, the elastic deformation of the vessel tissue accumulates continuously, and the friction head undergoes slight displacement, which is the presliding phenomenon [35]. When the contacting objects are in the presliding stage, the driving force must overcome the maximum shear force parallel to the contact interface, which is equivalent to the maximum static friction force. There is no relative sliding between the friction head and the vessel tissue interface, which is the viscous friction stage (Stage 1). When the COF reaches its maximum value of 0.0574, it is the maximum static COF, and the friction head continues to move into the slip friction stage (Stage 2), where the accumulated elastic deformation of the material gradually releases, causing relative sliding between the friction head and the vascular surface, and the COF first decreases and then stabilizes. In Stage 3, the COF curve fluctuates continuously, a process that involves elastic deformation of the material, which alternately accumulates and releases over time, resulting in a typical "stick–slip" phenomenon [36].

Figures 3(c)–3(e) show the changes in the COF, friction, and energy dissipation between the friction head and vascular tissue at various friction times. The friction and displacement curves during reciprocating motion form a closed curve, known as the "frictional loop", which is the frictional–displacement (F_f–D) curve. The area of this closed curve is equal to the energy consumed during the friction process between the friction head and vascular tissue, that is, the energy dissipated. Figure 3(c) shows the typical F_f–D curves of the first cycle (0 min), the 50th cycle (5 min), the 100th cycle (10 min), the 150th cycle (15 min), and the 200th cycle (20 min) of the friction experiment (velocity: 5 mm/s, normal force: 0.4 N). Owing to the nonlinear and viscoelastic properties of vascular tissue, the F_f–D curve becomes more irregular with increasing time, indicating that the initial friction interface has changed. Moreover, the energy dissipation gradually increases with increasing friction time, which is similar to the trend of the COF shown in Fig. 3(d). Within the first 5 min, the changes in the COF and energy dissipation are relatively small, indicating that the state of the friction interface is relatively stable. There is subsequently a significant increase in energy dissipation and the COF, which may be related to changes in the vascular tissue interface. This phenomenon is further discussed in Section 4.2, which examines the mapping relationship between friction factors and damage.

3.2 Dependence of the normal load

Figures 4(a)–4(e) present the typical F_f–D curves of the friction head and vascular tissue under different normal forces. All the curves exhibit an irregular rectangular shape within one reciprocating cycle. When the normal force is 0.2 N, the F_f–D curve remains stable within 20 min, and the corresponding energy dissipation changes very little, as shown in Fig. 4(g). With increasing normal force, the contact state between the friction head and vascular tissue gradually changes from sliding friction to "stick–slip" friction, indicating a change in the frictional interface. Moreover, frictional energy dissipation increases with increasing friction time under a single normal force. At the beginning of friction (0 min), the normal force has little effect on the COF, which is approximately 0.035. As time progresses, the COFs under different normal forces all increase, but the magnitudes of growth are not synchronous. The variation in the COF of the friction head in the first 10 min is consistent under a normal force of 0.2–0.8 N. As the friction time further increases, the differences in the COFs under different normal forces become more obvious; that is, the greater the normal force is, the more significant the change in the COF.

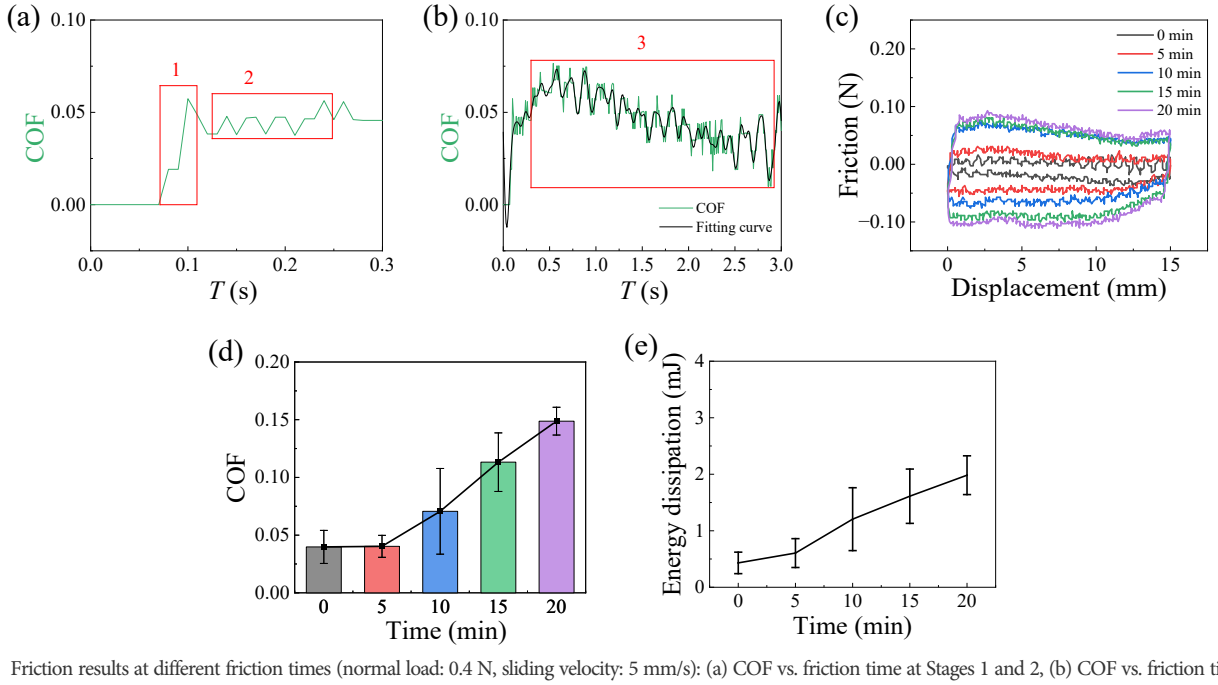

Fig. 3 Friction results at different friction times (normal load: 0.4 N, sliding velocity: 5 mm/s): (a) COF vs. friction time at Stages 1 and 2, (b) COF vs. friction time at Stage 3, (c) F_f–D curves at different times, (d) average COF at different times, and (e) average energy dissipation at different times.

清華大学出版社 Tsinghua University Press | SciOpen

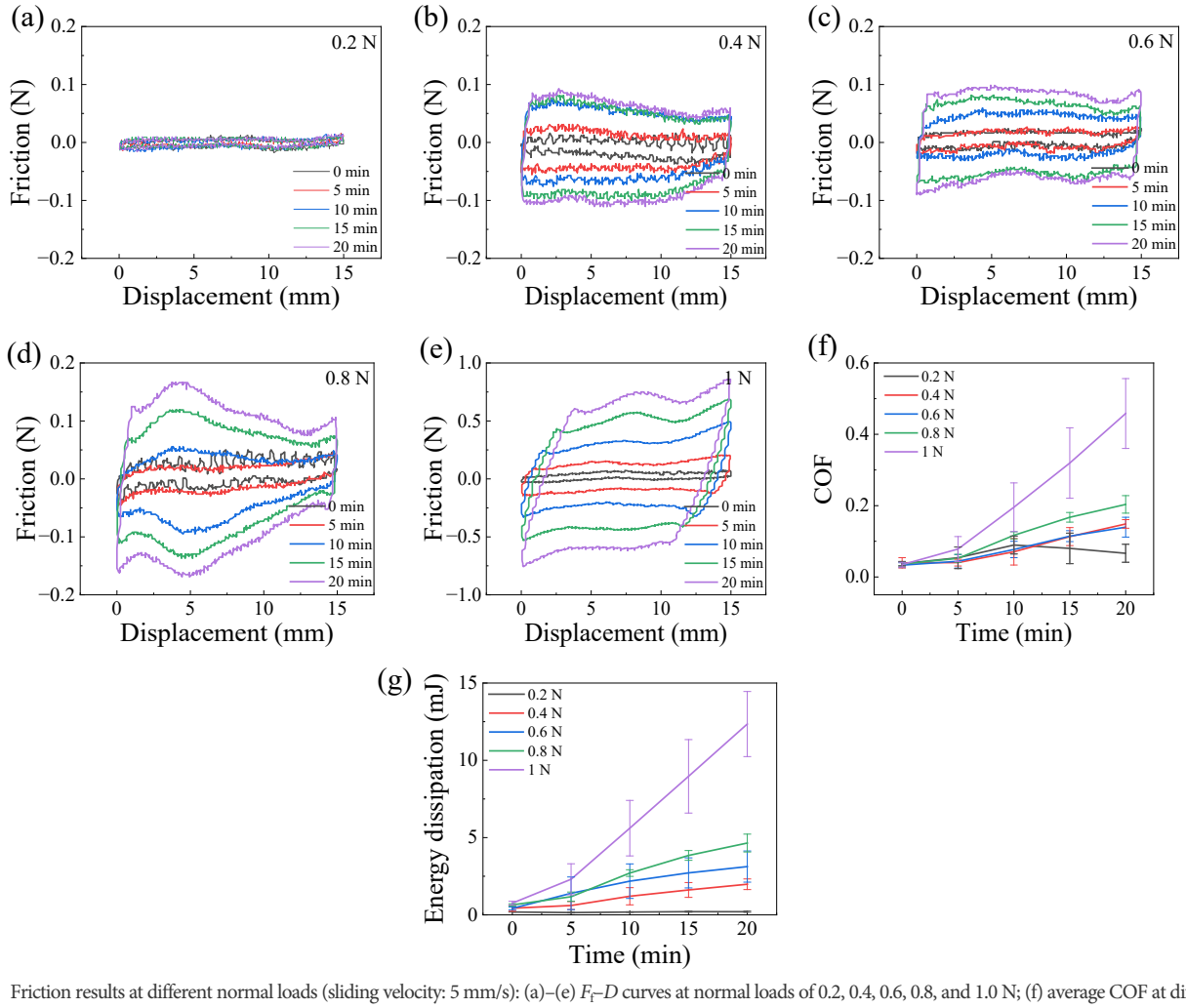

Fig. 4 Friction results at different normal loads (sliding velocity: 5 mm/s): (a)–(e) F_f–D curves at normal loads of 0.2, 0.4, 0.6, 0.8, and 1.0 N; (f) average COF at different normal loads; (g) average energy dissipation at different normal loads.

3.3 Dependence of the sliding velocity

Figures 5(a)–5(e) show that the F_f–D curves of the friction head and vascular tissue at different sliding velocities all exhibit an irregular rectangular shape. In the initial stage of friction (the first cycle, 0 min), the differences in frictional energy dissipation among different sliding velocities are relatively small but gradually become more evident as the number of cycles increases, as shown in Fig. 5(g). Particularly at a speed of 3 mm/s, the energy dissipation changes most drastically, with the F_f–D curve deviating the most from the initial rectangle in size and shape, indicating a significant change in the friction interface, where "stick–slip" friction dominates and the situation continues to deteriorate. At sliding velocities of 1 and 9 mm/s, the energy dissipation is the smallest, and their F_f–D curves change little with increasing number of cycles, indicating a relatively stable friction interface. The average COF also shows a similar trend. In the initial stage of friction, the influence of different sliding velocities on the friction coefficient is relatively small. However, as the number of cycles increases, the differences in the COFs among different sliding velocities become significantly greater (Fig. 5(f)). When the number of cycles reaches 200, the COF change is the smallest at a speed of 1 mm/s, whereas it is the largest at a speed of 3 mm/s. This trend indicates that the friction coefficient initially increases and then decreases as the velocity increases.

3.4 Injury characteristics of the vascular tissue

3.4.1 Surface damage

To explore the influence of friction behavior between the friction head and vascular tissue, SEM was used to examine the inner surface of the aorta. The SEM results for different friction times, normal forces, and sliding velocities are shown in Fig. 6. The vascular surface is not smooth or flat. However, instead of a protruding surface covered with pebble-like structures, which are the cytoplasmic protrusions of endothelial cells. From the SEM images at different frictional times in Fig. 6(a), it can be observed that the number of endothelial cells decreases continuously with increasing friction time, and they are no longer visible at 10 min. At the same time, strip-like rolled-up tissues begin to appear, and larger rolled-up tissues appear as the frictional time increases. The relationship between the diameter of the rolled-up tissues resulting from intimal rupture and the friction time was statistically analyzed, and the results are shown in Fig. 6(d). Similarly, changes in the vascular surface can be observed in friction experiments conducted under different normal loads and sliding velocities, as shown in Figs. 6(b) and 6(c). According to the statistical results in Figs. 6(e) and 6(f), with increasing normal force, the maximum diameter of the rolled-up tissues of the intima rupture increases, whereas the maximum diameter of the rolled-up tissues of the intima rupture first increases, reaches the maximum value at

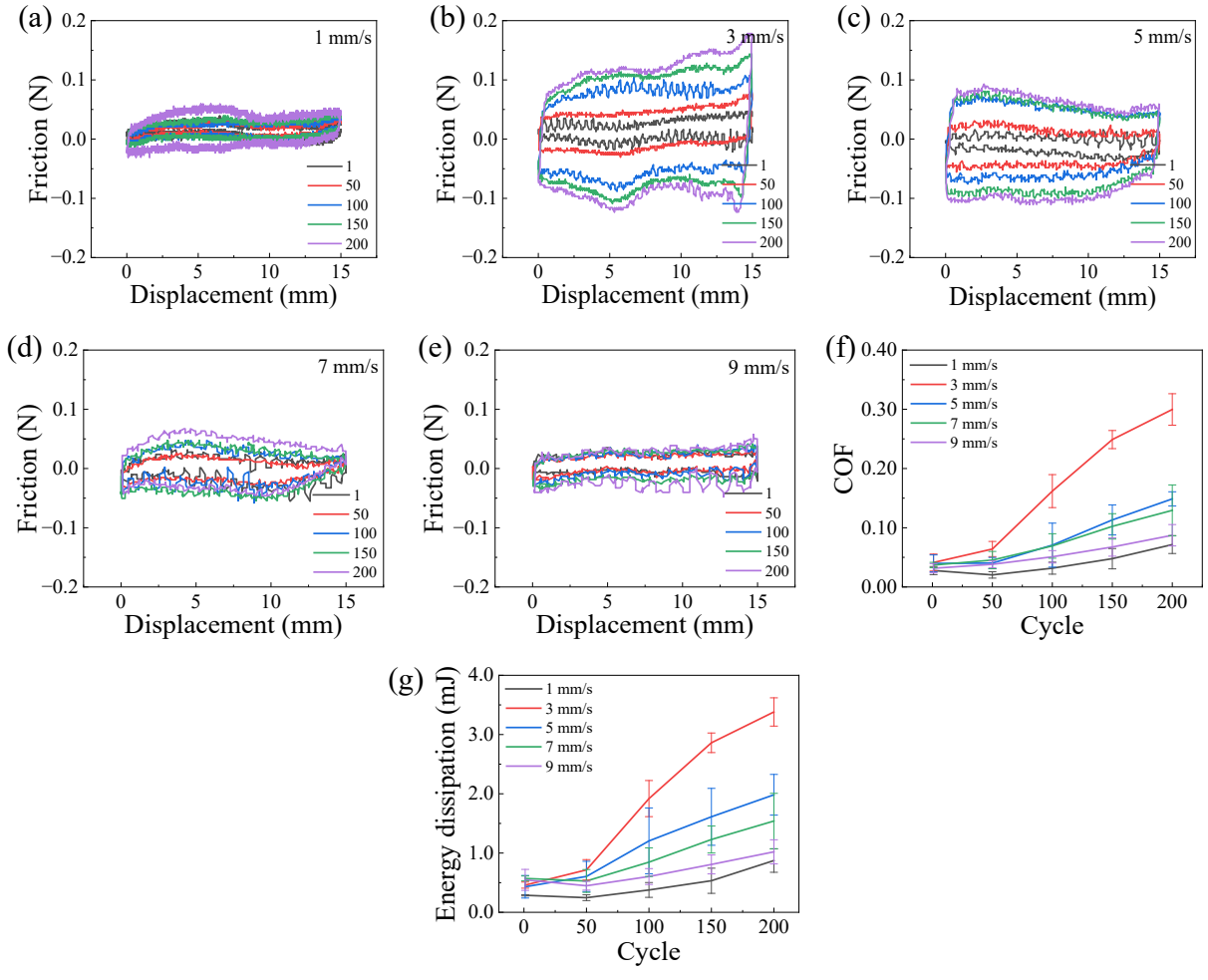

Fig. 5 Friction results at different sliding velocities (normal load: 0.4 N): (a)–(e) F_t–D curves at normal loads of 1, 3, 5, 7, and 9 mm/s; (f) average COF at different sliding velocities; (g) average energy dissipation at different sliding velocities.

3 mm/s, and then gradually decreases with increasing sliding velocity.

To further investigate the influence of different friction factors on the friction behavior between the friction head and vascular tissue, the intima surface was stained with fluorescence, and the distributions of cell nuclei (Fig. 7) and surface glycoproteins (Fig. 8) were statistically analyzed. Figure 7(a) shows that the shapes of the endothelial cell nuclei are relatively consistent, all presenting an elliptical shape, and are evenly distributed over the surface; however, their arrangement is not regular or uniform. Figures 7(d)–7(f) show that after 0.5 min of friction, the number of cell nuclei changed. Among them, the number of cell nuclei decreased by 25%, and this decrease was rapid with increasing friction time. When the friction time is 5 min, it is less than 30%, and then it remains relatively stable but gradually decreases. In the friction experiments with varying normal forces and moving speeds, the trend of increased damage to the number of cell nuclei is consistent with the change in the maximum diameter of the intima rolling-up tissue. On the other hand, the surface of blood vessels is covered with a layer of glycoprotein (glycocalyx), as shown in Figs. 8(a)–8(c), whose distribution is generally consistent with that of endothelial cells. After friction, the inner membrane glycoprotein is exposed on the surface, resulting in a significant difference in glycoprotein fluorescence intensity compared with that of the friction-free surface. The fluorescence intensity gradually decreased from 0.5 to 20 min. In contrast, the nonfriction sample exhibited a lower intensity of fluorescence (Fig. 8(d)). This might be because, in the complete vascular epithelium, the cells form a layered structure and are closely connected to each other, which can prevent the deep penetration of ConA dye. As a result, the detection rate of the unfrictional sample would be lower. However, friction can damage cells, loosening the cell-to-cell contact and increasing the permeability of the cell membrane [37]. For Fig. 8(e), except for the cases where the loading parameters are relatively small (0.2 N), i.e., where the friction damage to the vascular tissue is not severe, the overall trend of glycoproteins shows an overall downward trend. In Fig. 8(f), except for the cases where the sliding velocity is 1 mm/s, the overall trend of the change is consistent with that shown in Fig. 7(f) when the special points at 9 mm/s are ignored.

3.4.2 *Cross-sectional damage*

Figure 9 shows that the innermost layer of the aorta can be clearly distinguished as dark brown, granular endothelial cells closely adhering to the surface of the blood vessel. Next, the subendothelial layer, which appears as a red, spongy, fluffy structure, is mainly composed of loose connective tissue with collagen fibers interspersed with a small number of smooth muscle cells and elastic fibers. The endothelial cells and subendothelial layer together form the intima of the blood vessel. Outside the intima, there is an internal elastic lamina that appears black in EVG staining and is composed of elastic fibers, generally serving as the boundary between the intima and the media. The media of the aorta are composed mainly of elastic fibers and

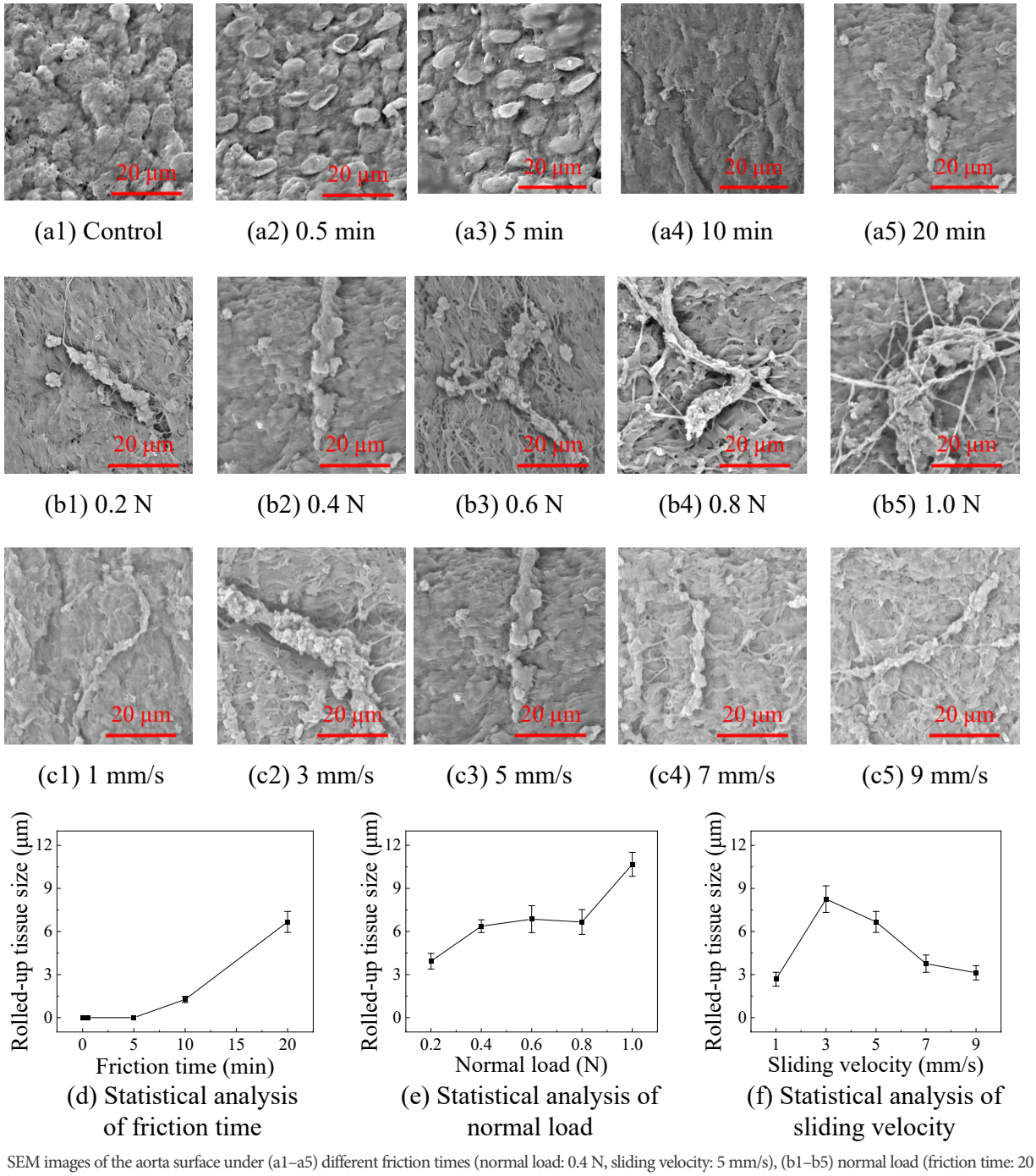

Fig. 6 SEM images of the aorta surface under (a1–a5) different friction times (normal load: 0.4 N, sliding velocity: 5 mm/s), (b1–b5) normal load (friction time: 20 min, sliding velocity: 5 mm/s), (c1–c5) sliding velocities (frictional cycle: 200, normal load: 0.4 N), and (d–e) the corresponding quantitative results.

smooth muscle. The elastic fibers primarily exist in the form of elastic membranes, and dozens of layers of these membranes can be observed in the figure, presenting a wavy shape. Smooth muscle cells and a small amount of collagen fibers are interspersed between the membranes. The outermost layer of the aorta is the adventitia, which is separated from the media by an external elastic lamina and consists mainly of loose connective tissue containing collagen fibers and elastic fibers.

The transverse sections of the aorta at different friction times are shown in Fig. 8(a). The adhesion of endothelial cells to the vascular surface was not as tight at 0.5 min, and some had detached. This phenomenon is more evident after 5 min. In addition to the detachment of endothelial cells, the subendothelial layer has transitioned from a smooth surface to a villous surface, indicating that friction damage has extended to the subendothelial layer. With increasing friction time, most of the endothelial cells disappeared by 10 min, and the structure of the subendothelial layer became looser, resulting in a reduction in thickness. At 20 min of friction, it was challenging to observe endothelial cells in these transverse sections, and the amount of loose connective tissue in the subendothelial layer significantly decreased. The changes in the intima thickness at different friction times indicate that the intima thickness gradually decreases with increasing friction time (Fig. 9(d)). From the tissue sections under different normal loads and moving speeds shown in Figs. 9(b) and 9(c), the relationship curves of the relative thickness of the intima can be obtained, as shown in Figs. 9(e) and 9(f). Under the most severe friction damage (normal force: 1 N), the internal elastic

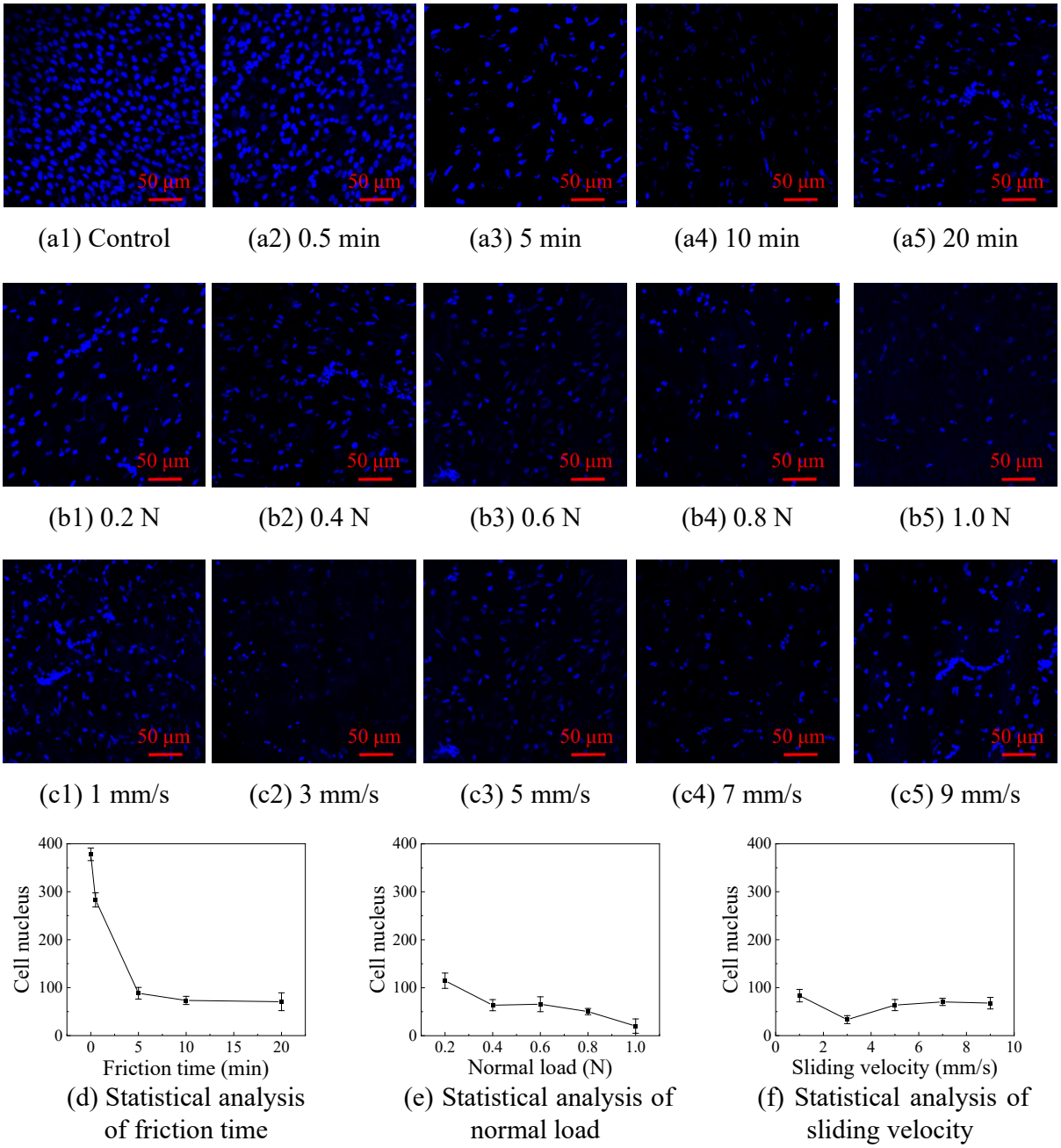

Fig. 7 DAPI fluorescence images of the aorta surface under different (a1–a5) friction times (normal load: 0.4 N, sliding velocity: 5 mm/s), (b1–b5) normal loads (friction time: 20 min, sliding velocity: 5 mm/s), and (c1–c5) sliding velocities (frictional cycle: 200, normal load: 0.4 N), and (d–f) the corresponding quantitative results.

membrane is exposed on the inner surface of the blood vessel but has not reached the middle layer of the blood vessel.

3.5 Tissue damage assessment system

3.5.1 Construction of the scoring system

The damage to blood vessels was evaluated through surface topography, fluorescence staining, and tissue sectioning. The main types of damage to vascular tissue include endothelial cell shedding, surface tissue curling, intimal wear, and changes in surface glycoproteins. On the basis of the tissue damage evaluation theory introduced in Section 2.5, a tissue damage scoring system was established on the basis of the above four types of damage to assess the degree of damage to vascular tissue (Table 3). The quantified data of the above four types of tissue damage were tested three times, and the average value±standard deviation was taken. The shedding of endothelial cells and intimal wear have upper and lower limit values, so these values were normalized into standardized data. With respect to the changes in surface glycoproteins and surface tissue curling, the range standardization method was employed to convert the quantified data into standardized data. The hierarchical analysis method was subsequently used to allocate the weights of the four damage types, as shown in Table 4. The degree of vascular tissue damage was scored according to Eqs. (2)–(5).

3.5.2 Analysis of assessment results

The degree of intimal injury is classified on the basis of the extent of vascular intimal damage as well as in Refs. [33, 34], as shown in Table 5. This injury scoring system can be widely applied to the evaluation of vascular intimal injury, especially for the biological safety analysis of vascular interventional devices, such as the

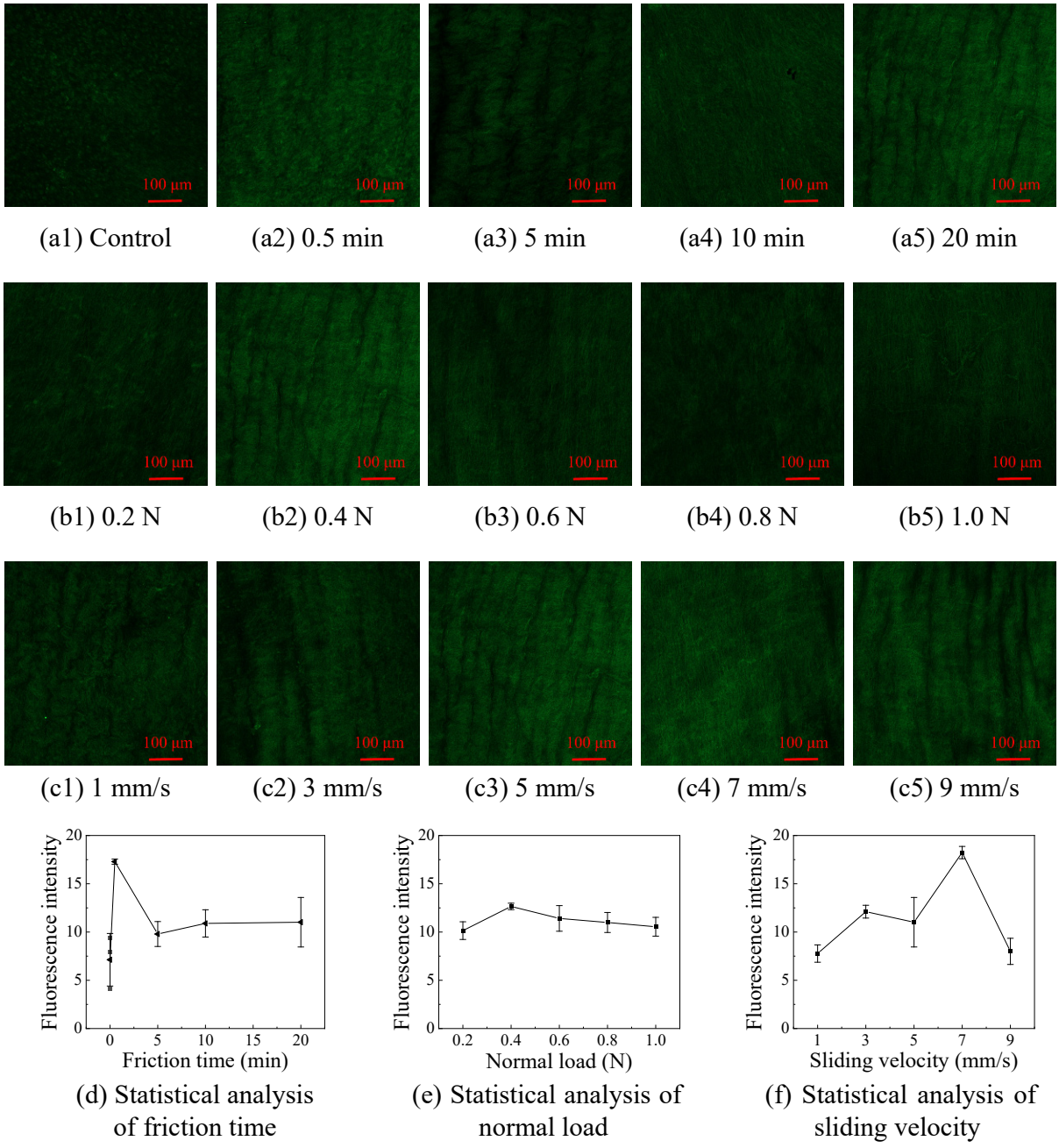

Fig. 8 ConA fluorescence staining images of the aorta surface under (a1–a5) different friction times (normal load: 0.4 N, sliding velocity: 5 mm/s), (b1–b5) normal loads (friction time: 20 min, sliding velocity: 5 mm/s), and (c1–c5) sliding velocities (frictional cycle: 200, normal load: 0.4 N), and (d–f) the corresponding quantitative results.

evaluation of coating lubrication and friction reduction performance. Figure 9 shows the relationship between the friction factors (friction time, normal force, and sliding velocity) and the score of the degree of intimal injury. The higher the injury score is, the more severe the intimal injury.

As shown in Fig. 10(a), the intimal injury score increases rapidly with increasing friction time, exhibiting a nonlinear trend. Only 0.5 min of friction can cause vascular injury to reach Grade 2, and it can cause vascular tissue to reach Grade 3 injury within 5–10 min of friction. After 20 min of friction, Grade 4 injury was reached. The longer the friction time is, the more severe the wear, which aligns with standard logic and supports the validity of this scoring system. Combined with the results in Section 3.1, the energy dissipation and COF increase significantly when the friction time reaches 5 min, confirming that Grade 3 injury has a significant effect on the friction interface. Additionally, the intimal injury score tends to increase as the normal force increases (Fig. 10(b)). The degree of vascular tissue injury gradually becomes more severe with increasing friction time and normal force, indicating a positive correlation. As shown in Fig. 10(c), when the friction time and the normal force are constant, the intimal injury score first increases with increasing speed, reaches a maximum value at 3 mm/s, and then decreases with increasing speed, which matches the trend of the COF. The relationship between injury and speed is not a simple linear relationship.

4 Discussion

4.1 Friction mechanism at the catheter–vascular tissue interface

During the friction process, frictional damage to the vascular

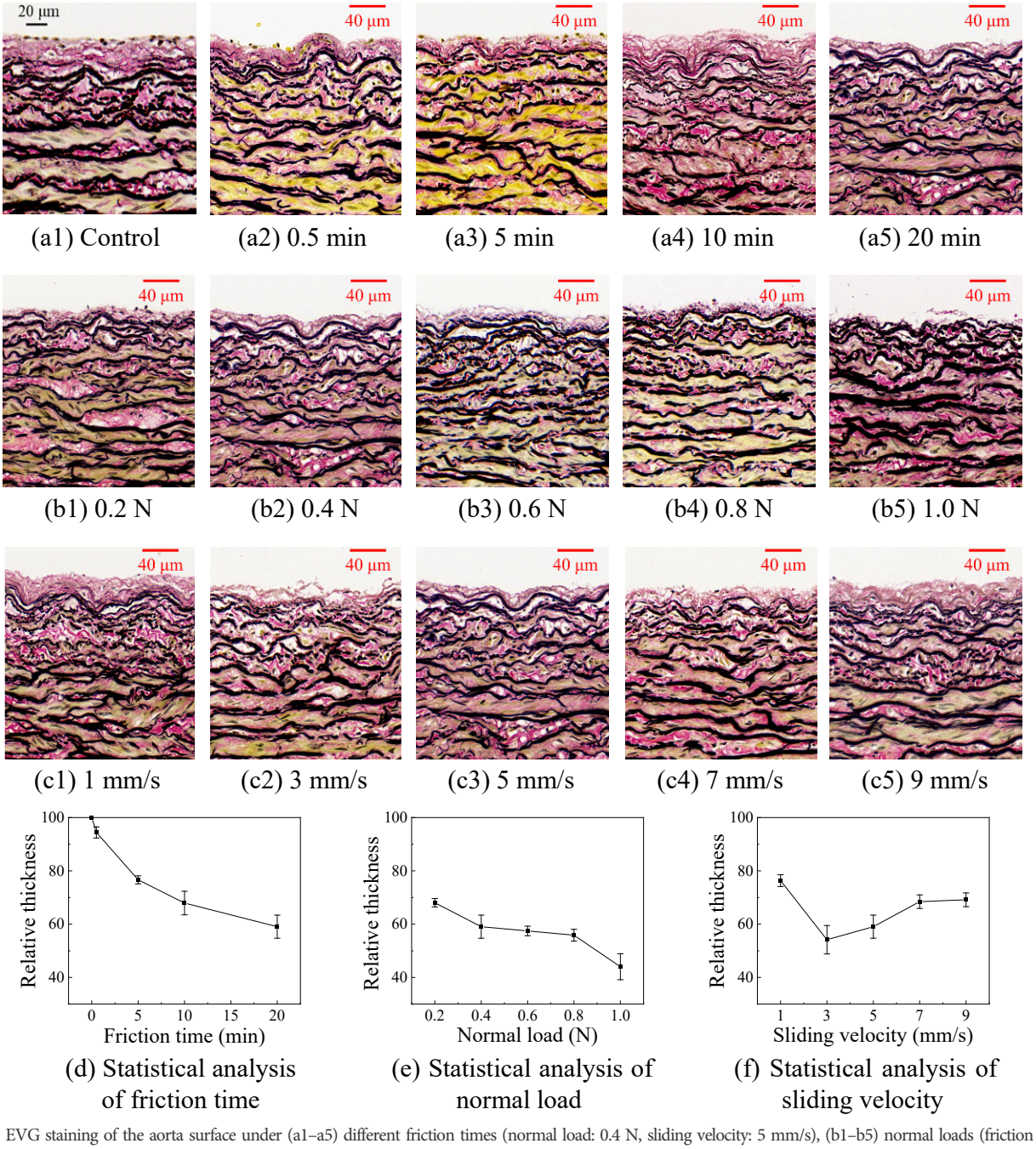

Fig. 9 EVG staining of the aorta surface under (a1–a5) different friction times (normal load: 0.4 N, sliding velocity: 5 mm/s), (b1–b5) normal loads (friction time: 20 min, sliding velocity: 5 mm/s)), and (c1–c5) sliding velocities (frictional cycle: 200, normal load: 0.4 N), and the corresponding quantitative results (d–e).

Table 3 Pathological scoring system for evaluating the degree of vascular tissue damage

Friction damage	Quantized data	Standardized data	Weight
Endothelial cells	Number of cell nuclei [a]	Z1	C1
Rolled-up tissue	Tissue size (μm) [b]	Z2	C2
Glycoprotein	Fluorescence intensity [c]	Z3	C3
Intimal thickness	Intimal thickness (μm) [d]	Z4	C4
Total	GI = C1 × Z1 + C2 × Z2 + C3 × Z3 + C4 × Z4		

Note: [a] The number of cell nuclei in a 200× field of view (320 μm × 320 μm); [b] the diameter of the largest tissue fold within a 5000× field of view; [c] the average fluorescence intensity within 100× field of view (640 μm × 640 μm); [d] the thickness of the inner membrane within a 40× field of view.

surface can lead to a series of noticeable tissue changes. First, the number of endothelial cells significantly decreases, and the glycoprotein layer, which serves a lubricating function, gradually disappears [17, 38]. Second, tissue curling occurs, further exacerbating the irregularity of the vascular surface. Additionally, the intimal thickness decreases, exposing collagen and elastic fibers, which also affects the mechanical properties of the vascular surface. Compared with the initial state, these changes in the

vascular surface undoubtedly represent significant deterioration. These changes not only alter the physical and chemical properties of the vascular surface but also influence the interaction at the friction interface. Therefore, as the friction head rubs against the vascular surface over time, the degree of vascular damage gradually increases, and the friction interface undergoes significant changes, resulting in variations in the friction coefficient. The relationships among these four factors are illustrated in Fig. 11.

When the normal force increases, the microprotrusions and microstructures on the surface of vascular tissue are subjected to greater compressive stress, causing the originally concave-convex structures to become smoother, thereby forming more contact points. This increase in the number of contact points not only leads to an increase in the contact area but also enhances the interaction between the friction interfaces, thereby intensifying the effect of the frictional force. Owing to the increase in frictional force, the degree of damage to the vascular surface also increases. Within the same friction time, the greater the normal force is, the more severe the damage to the vascular surface. In addition, the friction coefficient increases as the degree of damage increases, further exacerbating the vicious cycle of the friction process.

On the other hand, the frictional interface is in a mixed lubrication state under medium- and high-speed friction (3–9 mm/s), and the dynamic COF decreases with increasing relative motion speed, which conforms to the Stribeck characteristic curve [39]. However, the change in the friction coefficient is contrary to the Stribeck characteristic in the low-speed state (< 3 mm/s), which is consistent with the previous research results of our research group on esophageal tissue friction [40]. At lower speeds, most of the energy can be recovered through deformation due to the limited energy loss from hysteresis friction. As the speed gradually increases, the stress relaxation effect becomes less pronounced, and the vascular tissue cannot respond in time, resulting in an increase in hysteresis friction, which in turn leads to an increase in energy dissipation. Therefore, the COF increases with increasing speed. Additionally, the glycocalyx layer on the surface of vascular tissue can alter the path of the Stribeck characteristic curve, and the contact interface in the low-speed state remains in a mixed lubrication state [41].

Figure 7 shows a decrease in the number of nuclei with increasing damage, namely, friction time and normal load, which presents an opposite trend to that reported in other publications [37]. On the one hand, the vascular endothelium itself is composed of cells, as shown in Fig. 2(b), to which the dye DAPI can react directly. As we proceed further, the inner lining of the blood vessel tissue is mainly composed of red collagen fibers. In most cases, the EVG staining results indicate that frictional damage to the vascular surface is characterized primarily by

Table 4 Weight calculation table

Comparison matrix	Endothelial cells	Rolled-up tissue	Glycoprotein	Intimal thickness	Weight	CI [a]
Endothelial cells	1	3	5	3	0.513	0.089 < 0.1
Rolled-up tissue	1/3	1	3	1/3	0.150	
Glycoprotein	1/5	1/3	1	1/3	0.076	
Intimal thickness	1/3	3	3	1	0.261	

Note: [a] Coincidence indicator.

Table 5 Damage to the vascular intima

Damage level	Damage degree	Damage marker
Undamaged	0	The glycoprotein is evenly distributed and intact; the endothelial cells completely cover the inner membrane surface.
Grade 1	0–20%	Most retention of the endothelial cells.
Grade 2	20%–40%	Partial retention of endothelial cells.
Grade 3	40%–60%	The endothelial cells are almost completely lost, and the curled tissues are less than 5 μm in size.
Grade 4	60%–80%	There are some curled tissues with a diameter greater than 5 μm.
Grade 5	⩾ 80%	The diameter of the curled tissues is greater than 10 μm, and the internal elastic membrane is exposed.

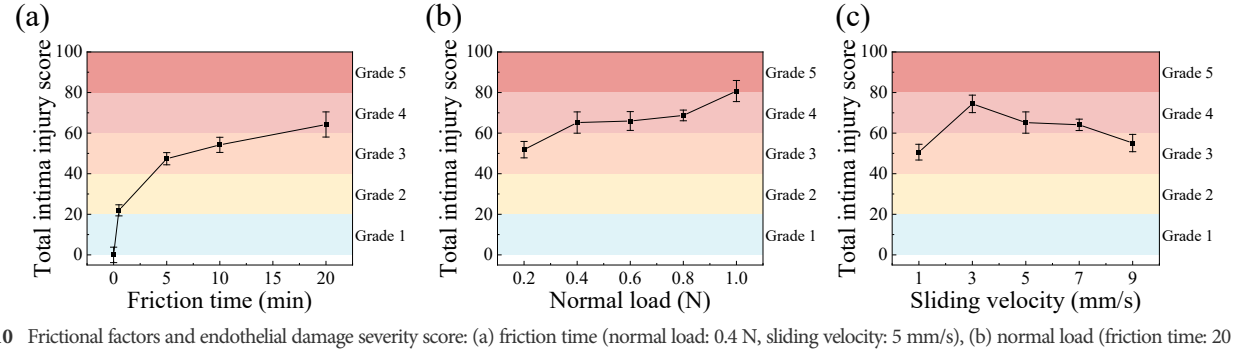

Fig. 10 Frictional factors and endothelial damage severity score: (a) friction time (normal load: 0.4 N, sliding velocity: 5 mm/s), (b) normal load (friction time: 20 min, sliding velocity: 5 mm/s), and (c) sliding velocity (frictional cycle: 200 cycles, normal load: 0.4 N).

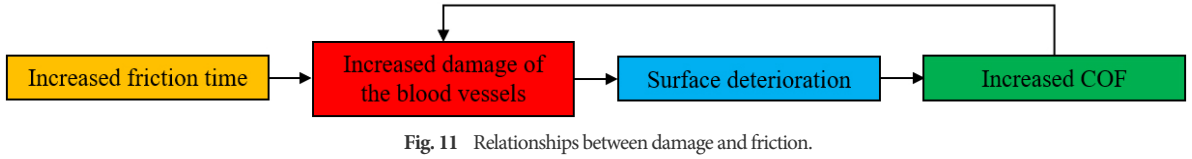

Fig. 11 Relationships between damage and friction.

changes in endothelial cells and elastic fibers. In extreme cases (1.0 N), the red collagen fibers are erased (Fig. 9(b5)). Therefore, the number of cell nuclei tends to decrease as damage increases [27, 29].

In addition, a quantitative evaluation of mechanical damage to vascular tissues, such as the small intestine [34], liver tissue [42], gallbladder tissue [43], airway tissue [44, 45], and colon tissue [46], was performed for the first time, and the relationships between mechanical factors and the degree of damage were explored. The similarity is that both systems assess the degree of mechanical damage to the organization. However, the current system does not directly score the damage before summarizing and processing it. Instead, typical damage characteristics are quantified through data standardization and weighted processing, ultimately obtaining comprehensive damage information that avoids subjective factors as much as possible. Compared with the Hematoxylin and Eosin (H&E) staining methods used in previous studies for evaluating vascular tissue clamping force [47], this study adopted four different types of damage for quantitative analysis. It aims to include as much information about tissue damage as possible to ensure the accuracy of the data.

4.2 Correlation analysis between the friction coefficient and damage score

This work uses Origin software to conduct a Pearson correlation analysis on the COF and damage score results under various friction times, normal forces, and moving speeds to explore the relationships among them. The Pearson correlation coefficient, as a statistical magnitude of the strength and direction of a linear relationship, ranges from −1 to 1. A positive or negative value of the Pearson correlation coefficient indicates the direction of the correlation between two sets of data, with a positive value indicating a positive correlation and a negative value indicating a negative correlation. The absolute value of the coefficient reflects the strength of the correlation (generally, less than 0.2: no correlation; 0.2–0.4: weakly correlated; 0.4–0.6: moderately correlated; 0.6–0.8: strongly correlated; and greater than 0.8: highly correlated). As shown in Table 6, the correlation analysis between the COF and the vascular injury score revealed a strong correlation between the friction coefficient and the injury score. The correlation coefficients between the friction coefficient and the injury score caused by the friction time, normal force, and speed are all greater than 0.6, indicating a strong correlation or greater. The correlation between the normal load and sliding velocity even reaches a high degree of correlation. This suggests a close connection between the friction effect and tissue surface damage.

5 Conclusions

This study investigated the frictional characteristics of the PTFE friction head and porcine aortic vessels under varying friction factors through in vitro tissue friction experiments. Multiple methods have been used to analyze the vascular damage caused by friction. On the basis of the experimental results, a damage evaluation system was established, and a mapping relationship between the interaction mechanism of catheters and vessels under different motion conditions and the tissue injury mechanism was constructed. The main conclusions of this paper are as follows.

(1) During the friction process, the friction coefficient fluctuated, indicating a typical "stick–slip" phenomenon. The frictional force and energy dissipation increased over time, especially significantly after 5 min. The F_f–D curves become irregular over time, reflecting the changes in the friction interface.

(2) As the normal force increased, the COF and energy dissipation between the friction head and vascular tissue also increased. In contrast, the COF and energy dissipation first tend to increase but then decrease at varying speeds.

(3) A quantitative evaluation system for vascular tissue injury was established according to indicators such as endothelial cells, glycoproteins, curled tissues, and intimal thickness on the vascular surface. On the basis of this system, damage scores and damage grades were assigned to vascular surface injuries in friction experiments.

(4) The aggravation of vascular damage intensifies the irregularity of the vascular surface, affecting its mechanical properties and thus leading to significant changes in the friction interface. Pearson correlation analysis revealed that the COF and the injury score were strongly correlated, and the correlation between the normal load and sliding velocity was even greater than that between the friction time and the injury score.

Table 6 Correlation coefficient analysis table

COF-damage score	Total	Friction time	Normal load	Sliding velocity
P	0.0060 (**)	0.2035	0.0181 (*)	0.0222 (*)
Relevance	0.6724	0.6833	0.9386	0.9297

Acknowledgements

This work was supported by the National Natural Science Foundation of China (No. 52205186).

Declaration of competing interest

The authors have no competing interests to declare that are relevant to the content of this article.

Electronic Supplementary Material

Supplementary material is available in the online version of this article at https://doi.org/10.26599/FRICT.2025.9441194.

References

[1] Mensah G A, Roth G A, Fuster V. The global burden of cardiovascular diseases and risk factors. *J Am Coll Cardiol* **74**(20): 2529–2532 (2019)

[2] Yuan H L, Lin C X, Wang C Y. Research progress of the interaction between blood vessels and intervention catheters and its surface modification. *Friction* **13**(7): 9441003 (2025)

[3] Timmis A, Vardas P, Townsend N, Torbica A, Katus H, De Smedt D, Gale C P, Maggioni A P, Petersen S E, Huculeci R. European Society of Cardiology: Cardiovascular disease statistics 2021: Executive Summary. *Eur Heart J* **8**(4): 377–382 (2022)

[4] Zyriax B C, Windler E. Lifestyle changes to prevent cardio- and cerebrovascular disease at midlife: A systematic review. *Maturitas* **167**: 60–65 (2023)

[5] Ratner B D. The catastrophe revisited: Blood compatibility in the 21st century. *Biomaterials* **28**(34): 5144–5147 (2007)

[6] Sobolewski P, El Fray M. Cardiac catheterization: Consequences for the endothelium and potential for nanomedicine. *WIREs Nanomed Nanobi* **7**(3): 458–473 (2015)

[7] Dellimore K H, Franklin S E, Helyer A R. A review of catheter related complications during minimally invasive transcatheter cardiovascular intervention with implications for catheter design. *Cardiovasc Eng Techn* **5**(3): 217–232 (2014)

[8] Şahin B, İlgün G. Risk factors of deaths related to cardiovascular diseases in World Health Organization (WHO) member countries. *Health Soc Care Comm* **30**(1): 73–80 (2022)

[9] Ma L Y, Wang Z W, Fan J. An essential introduction to the annual report on cardiovascular health and diseases in China. *Chinese General Practice* **25**(27): 3331 (2022) (in Chinese)
[10] Takashima K, Ohta M, Yoshinaka K, Washio T, Chinzei K. Methods for evaluating friction between intravascular device and vascular biomodel. *Tribol Online* **19**(1): 42–54 (2024)
[11] Li P, Feng J, Zhang X, Fang D L, Zhang J X, Liang C M. Modeling and experimental study of the intervention forces between the guidewire and blood vessels. *Med Eng Phys* **127**(1): 104166 (2024)
[12] Wagner R M F, Maiti R, Carré M J, Perrault C M, Evans P C, Lewis R. Bio-tribology of vascular devices: A review of tissue/device friction research. *Biotribology* **25**: 100169 (2021)
[13] Takashima K, Shimomura R, Kitou T, Terada H, Yoshinaka K, Ikeuchi K. Contact and friction between catheter and blood vessel. *Tribol Int* **40**(2): 319–328 (2007)
[14] Prokopovich P, Perni S, Piccirillo C, Pratten J, Parkin I P, Wilson M. Frictional properties of light-activated antimicrobial polymers in blood vessels. *J Mater Sci-Mater M* **21**(2): 815–821 (2010)
[15] Prokopovich P, Perni S. Contact interactions of aorta against PVC catheters. *Tribol Int* **66**: 157–164 (2013)
[16] Bostan L E, Noble C, Smulders N, Lewis R, Carré M J, Franklin S, Green N H, MacNeil S. Measurement of friction-induced changes in pig aorta fibre organization by non-invasive imaging as a model for detecting the tissue response to endovascular catheters. *Biotribology* **12**: 24–32 (2017)
[17] Lin C X, Kaper H J, Li W, Splinter R, Sharma P K. Role of endothelial glycocalyx in sliding friction at the catheter-blood vessel interface. *Sci Rep-UK* **10**: 11855 (2020)
[18] Wang Z X, Wang K P, Xu Y. Friction injury of the central vein caused by catheter for hemodialysis: An *in vitro* study. *Sci Rep-UK* **14**: 5836 (2024)
[19] Dunn A C, Zaveri T D, Keselowsky B G, Sawyer W G. Macroscopic friction coefficient measurements on living endothelial cells. *Tribol Lett* **27**(2): 233–238 (2007)
[20] Xia T, Yu J C, Du M, Chen X M, Wang C B, Li R B. Vascular endothelial cell injury: Causes, molecular mechanisms, and treatments. *MedComm* **6**(2): 70057 (2025)
[21] Dong Z F, Long Y, Sun W J, Wang Y, Huang Y H, Wang G X, He B, Yin T Y. Role of smooth muscle progenitor cells in vascular mechanical injury and repair. *Med Nov Technol Devices* **16**: 100178 (2022)
[22] Park H M, Kim C L, Kong D, Heo S H, Park H J. Innovations in vascular repair from mechanical intervention to regenerative therapies. *Tissue Eng Regen Med* **22**(4): 551–567 (2025)
[23] Gao F R, Xiong C H, Xiong Y L. Mechanical damage evaluation of living tissue in vascular therapy. *Lect Notes Artif Int*: 607–616 (2008)
[24] Dellimore K H J, Mank A J G, Wojnowski J, Noble C, Franklin S E. Evaluation of catheter-induced tribological damage to porcine aorta using infra-red spectroscopy. *Biotribology* **7**: 11–21 (2016)
[25] Cheheltani R, McGoverin C M, Rao J, Vorp D A, Kiani M F, Pleshko N. Fourier transform infrared spectroscopy to quantify collagen and elastin in an *in vitro* model of extracellular matrix degradation in aorta. *Analyst* **139**(12): 3039–3047 (2014)
[26] Votteler M, Carvajal Berrio D A, Pudlas M, Walles H, Stock U A, Schenke-Layland K. Raman spectroscopy for the non-contact and non-destructive monitoring of collagen damage within tissues. *J Biophotonics* **5**(1): 47–56 (2012)
[27] Lin C X, Wan H P, Kaper H J, Sharma P K. A hyaluronic acid based lubricious coating for cardiovascular catheters. *Tribol Int* **151**: 106495 (2020)
[28] Wan H P, Lin C X, Kaper H J, Sharma P K. A polyethylene glycol functionalized hyaluronic acid coating for cardiovascular catheter lubrication. *Mater Design* **196**: 109080 (2020)
[29] Lin C X, Huang Z Y, Wu T T, Zhou X T, Zhao R F, Xu Z B. A chitosan and hyaluronic acid-modified layer-by-layer lubrication coating for cardiovascular catheter. *Colloid Surface B* **217**: 112687 (2022)
[30] Hofmann G, Jubin P, Gerligand P, Gallois-Bernos A, Franklin S, Smulders N, Gerhardt L C, Valster S. *In-vitro* method for determining corneal tissue friction and damage due to contact lens sliding. *Biotribology* **5**: 23–30 (2016)
[31] Radovic M, Ghalwash M, Filipovic N, Obradovic Z. Minimum redundancy maximum relevance feature selection approach for temporal gene expression data. *BMC Bioinformatics* **18**: 9 (2017)
[32] Saaty T L. *Fundamentals of Decision Making and Priority Theory with the Analytic Hierarchy Process*. London (UK): RWS Publications, 1994.
[33] Wang J, Ma L, Li W, Zhou Z R. Influence of different lubricating fluids on friction trauma of small intestine during enteroscopy. *Tribol Int* **126**: 29–38 (2018)
[34] Wang J, Li W, Wang B R, Zhou Z R. Influence of clamping parameters on the trauma of rabbit small intestine tissue. *Clin Biomech* **70**: 31–39 (2019)
[35] Song B J, Yan S Z. Research progress on interface stick–slip friction phenomenon. *China Mechanical Engineering* **28**(13): 1513–1522 (2017) (in Chinese)
[36] Kwiatkowska M, Franklin S E, Hendriks C P, Kwiatkowski K. Friction and deformation behaviour of human skin. *Wear* **267**(5–8): 1264–1273 (2009)
[37] Barros R C, Van Kooten T G, Veeregowda D H. Investigation of friction-induced damage to the pig cornea. *Ocul Surf* **13**(4): 315–320 (2015)
[38] Kuo J C, Gandhi J G, Zia R N, Paszek M J. Physical biology of the cancer cell glycocalyx. *Nat Phys* **14**(7): 658–669 (2018)
[39] Hutchings I M. Tribology: Friction and wear of engineering materials. *Mater Design* **13**(3): 187 (1992)
[40] Lin C X, Yu Q Y, Wang J, Ji W, Li W, Zhou Z R. Friction behavior between endoscopy and esophageal internal surface. *Wear* **376**: 272–280 (2017)
[41] Lievens C W, Rayborn E. Tribology and the ocular surface. *Clin Ophthalmol* **16**: 973–980 (2022)
[42] Wang J, Yu Q Y, Li W, Wang B R, Zhou Z R. Influence of clamping stress and duration on the trauma of liver tissue during surgery operation. *Clin Biomech* **43**: 58–66 (2017)
[43] Marucci D D, Shakeshaft A J, Cartmill J A, Cox M R, Adams S G, Martin C J. Grasper trauma during laparoscopic cholecystectomy. *Aust NZ J Surg* **70**(8): 578–581 (2000)
[44] Wang C, Zhao R, Liu W, Di L N, Zhao X Z, Rong Y H, Ning F G, Zhang G A. Pathological changes of the three clinical types of laryngeal burns based on a canine model. *Burns* **40**(2): 257–267 (2014)
[45] Zhao R, Di L N, Zhao X Z, Wang C, Zhang G A. Measuring surface temperature and grading pathological changes of airway tissue in a canine model of inhalational thermal injury. *Burns* **39**(4): 767–775 (2013)
[46] Barrie J, Russell L, Hood A J, Jayne D G, Neville A, Culmer P R. An *in vivo* analysis of safe laparoscopic grasping thresholds for colorectal surgery. *Surg Endosc* **32**(10): 4244–4250 (2018)
[47] Famaey N, Verbeken E, Vinckier S, Willaert B, Herijgers P, Vander Sloten J. *In vivo* soft tissue damage assessment for applications in surgery. *Med Eng Phys* **32**(5): 437–443 (2010)

Chengxiong Lin received his Ph.D. degree in mechanical design and theory from Southwest Jiaotong University, China, in 2020. He is an associate professor from the School of Mechanical Engineering at Wuhan University of Science and Technology, China. His research interests include biotribology, bio 3D printing, and antibacterial lubricating materials.

Huilu Yuan received his bachelor and master degrees in electromechanical engineering from Guangdong University of Technology, China, in 2021. His research interests include surface engineering and medical devices.

Chengyong Wang received his Ph.D. degree from Dalian University of Technology, China, in 1989. He is a professor and director of the Guangdong Provincial Key Laboratory of Minimally Invasive Surgical Instruments and Manufacturing Technology, Guangdong University of Technology, China. His research interests include machining difficult-to-machine materials and the design and manufacture of medical and surgical tools.